

Radiative Fallo in Neutron Star Spacetimes

Vasiliki Pavlidou¹, Konstantinos Tassis¹, Thomas W. Baumgarte², and Stuart L. Shapiro^{1,2,3}

¹ Department of Astronomy, University of Illinois at Urbana-Champaign, Urbana, IL 61801

² Department of Physics, University of Illinois at Urbana-Champaign, Urbana, IL 61801

³ NCSA, University of Illinois at Urbana-Champaign, Urbana, IL 61801

We systematically study late-time tails of scalar waves propagating in neutron star spacetimes. We consider uniform density neutron stars, for which the background spacetime is analytic and the compaction of the star can be varied continuously between the Newtonian limit $2M/R \rightarrow 1$ and the relativistic Buchdahl limit $2M/R = 8/9$. We study the reflection of a finite wave packet of neutron stars of different compactness $2M/R$ and find that a Newtonian, an intermediate, and a highly relativistic regime can be clearly distinguished. In the highly relativistic regime, the reflected signal is dominated by quasi-periodic peaks, which originate from the wave packet bouncing back and forth between the center of the star and the maximum of the background curvature potential at $R = 3M$. Between these peaks, the field decays according to a power-law. In the Buchdahl limit $2M/R \rightarrow 8/9$ the light travel time between the center and the maximum of the curvature potential grows without bound, so that the first peak arrives only at infinitely late time. The modes of neutron stars can therefore no longer be excited in the ultra-relativistic limit, and it is in this sense that the late-time radiative decay from neutron stars loses all its features and gives rise to power-law tails reminiscent of Schwarzschild black holes.

I. INTRODUCTION

The late-time radiative falloff in a black hole spacetime was first studied with the goal of understanding how, in the absence of rotation, a spherically symmetric Schwarzschild black hole emerges in a general aspherical collapse. The first numerical results by de la Cruz, Chase and Israel [1] were followed up by the perturbative analytic study by Price [2], who showed that scalar, electromagnetic and gravitational radiation all decay as an inverse power of time. This late-time behavior is commonly referred to as "power-law tails".

The analysis of Gundlach, Price and Pullin [3] showed that power-law tails arise from backscattering off the weak gravitational potential in the far zone (cf. [4]). One immediate implication, namely that the late time behavior should be different in black hole spacetimes which are not asymptotically flat, was confirmed by Brady, Chambers, Krivan and Laguna [5], and later Brady, Chambers, Laarakkers and Poisson [6]. These authors studied radiative falloff in Schwarzschild-de Sitter spacetimes, and found that for nonspherical (and minimally coupled) perturbations, the power-law decay at early times changed into an exponential decay after a cosmological horizon timescale [7]. Another implication is that power-law tails should be present even in the absence of event horizons, e.g. for perturbations of neutron stars.

Perturbations of nonrotating, spherically symmetric relativistic neutron stars have been studied by many authors, mostly with the goal of finding their oscillation modes [8,16]. Typically, these modes are determined by assuming a time-dependence $\exp(i\omega t)$ and then studying the time-independent problem. The perturbation equations then reduce to an eigenvalue problem, which can be solved for the complex frequencies. In addition to

families of modes corresponding to those of Newtonian stars, relativistic stars also have modes which are reminiscent of the quasinormal modes of black holes and can be associated with the dynamical degrees of freedom of the gravitational field. Because of their association with gravitational waves, these modes are usually referred to as w -modes. Several distinct families of w -modes, both in axial and polar parity, have been found in numerical calculations (see the recent review by Kokkotas and Schmidt, [17]): curvature modes exist for all compactness $2M/R$, where M is the stellar mass and R the circumferential radius, trapped modes only arise in sufficiently compact stars with $2M/R > 2.3$, when radiation can be "trapped" inside the maximum of the background curvature potential at $R = 3M$ (see below), and interface modes are associated with a discontinuity of the background curvature at the surface of the star.

Similar to black holes, the response of a neutron star to a general perturbation will be a superposition of fluid and gravitational wave modes and a power-law tail. Since all modes decay exponentially, the late-time falloff should be dominated by the power-law tail. Unlike the quasinormal modes of a black hole, however, the frequency of the neutron star's w -modes depends on the compactness $2M/R$ of the star. As the compactness approaches the ultrarelativistic Buchdahl limit $2M/R = 8/9$ [18], the imaginary part of the frequency of at least some of these modes approaches zero, implying that their damping time becomes infinite [16,17]. A similar behavior had earlier been identified by Detweiler for the fluid modes (f-modes) of relativistic stars [9]. This observation immediately raises the question how a neutron star in the ultrarelativistic limit responds to a general perturbation, whether a power-law tail emerges, and whether its characteristic radiative falloff approaches that of a black

hole. In this paper we seek to answer this question by dynamically evolving the time-dependent perturbation equations.

So far, few authors have studied perturbations of relativistic stars by dynamically evolving the time-dependent perturbation equations, as opposed to assuming a $\exp(i t)$ time-dependence and solving the time-independent equations. Andersson and Kokkotas [19] studied the excitation of w -modes by an impinging gravitational wave, and discussed the prospect of detections by future gravitational-wave laser interferometers. Allen, Andersson, Kokkotas and Schutz [20] analyzed the spectrum of excited fluid and wave modes arising from several different sets of initial data. In some of these simulations, both the quasi-normal modes and subsequent power-law tails were observed (see [19], also Fig. 5 in [17]). Ruoff [21] generalized earlier results and included realistic equations of state.

In this paper, we dynamically evolve a scalar field in a neutron star background. We model the neutron star as a homogeneous, incompressible sphere, for which the background metric is known analytically. We derive an analytical generalized tortoise coordinate, which brings the equations into a particularly simple form. We then vary the compaction of the star between the Newtonian limit $2M/R \rightarrow 1$ and the Buchdahl limit $2M/R = 8/9$. Interestingly, the generalized tortoise coordinate distance between the center and the surface of the star diverges in the Buchdahl limit, implying that the light travel time becomes infinite.

We then study the reflection of finite wave packets off neutron stars of various compactness, and identify three distinct regimes: In the Newtonian regime $2M/R \rightarrow 1$, we find a reflection of the initial pulse from the center of the star, and a subsequent power-law falloff. In an intermediate regime, so-called trapped modes of the neutron star are excited and decay exponentially (see also [19, 21]). After these modes have decayed to sufficiently small values, the late-time tail re-emerges as a power-law. In this paper we focus on the highly relativistic regime, in which the wave packet bounces back and forth between the center of the star and the maximum of the background curvature potential at $R = 3M$, giving rise to quasi-periodic peaks in the reflected signal. Between these peaks, the field again decays according to a power-law. In the Buchdahl limit $2M/R \rightarrow 8/9$ the light travel time between the center and the maximum or the curvature potential grows without bound, so that the first peak arrives only at infinitely late time. The modes of neutron stars can therefore no longer be excited in the ultra-relativistic limit, and it is in this sense that tails from neutron stars lose all their features and give rise to power-law tails.

The paper is organized as follows. In Sec. II we introduce the basic equations, starting with a general spherically symmetric spacetime, then specializing to homogeneous neutron stars, and describing our numerical implementation of the equations. We discuss our numerical results and present characteristic examples for each of three different compaction regimes in Sec. III. In Sec. IV we briefly summarize our findings. We also include an appendix containing the derivation of a conserved energy integral of the motion, which we use as a numerical check.

The paper is organized as follows. In Sec. II we introduce the basic equations, starting with a general spherically symmetric spacetime, then specializing to homogeneous neutron stars, and describing our numerical implementation of the equations. We discuss our numerical

results and present characteristic examples for each of three different compaction regimes in Sec. III. In Sec. IV we briefly summarize our findings. We also include an appendix containing the derivation of a conserved energy integral of the motion, which we use as a numerical check.

II. BASIC EQUATIONS

A. Scalar Waves in Spherical Symmetry

In spherical symmetry, the line element can be written

$$ds^2 = -e^2 dt^2 + e^2 dr^2 + r^2(d\theta^2 + \sin^2\theta d\phi^2); \quad (1)$$

The wave equation for a massless and minimally coupled scalar field ϕ ,

$$\square \phi = g^{\mu\nu} \nabla_\mu \nabla_\nu \phi = 0; \quad (2)$$

can then be written

$$e^2 \left(\partial_{tt} + \frac{e^{(+)}}{r^2} \partial_r^2 \right) \phi + \frac{V^{(+)}(r)}{r^2} \phi = 0; \quad (3)$$

where we have decomposed the angular part of ϕ into the spherical harmonics $\phi(t; r; \theta; \phi) = \psi(t; r) Y_{lm}(\theta; \phi)$.

Introducing a "generalized tortoise coordinate" r^* satisfying

$$\frac{dr}{dr^*} = e^{-1}; \quad (4)$$

and substituting

$$\psi = r \chi \quad (5)$$

into eq. (3) yields

$$\partial_{tt} \chi + \partial_{r^* r^*} \chi = V_-(r) \chi; \quad (6)$$

where the effective potential $V_-(r)$ is given by

$$V_-(r) = e^2 \left(\frac{V^{(+)}(r)}{r^2} + \frac{e^{(+)}}{r} \right); \quad (7)$$

B. Uniform Density Neutron Stars

We now specialize to a constant density neutron star, for which

$$e = \begin{cases} \frac{3}{2} \left(1 - \frac{2M}{R} \right)^{1/2} \left(1 - \frac{2M}{R^3} r^2 \right)^{1/2} & r < R \\ \frac{2M}{r} & r > R \end{cases} \quad (8)$$

and

$$e^{-\lambda} = \begin{cases} 1 - \frac{2M}{R^3} r^2 & r < R \\ 1 - \frac{2M}{r} & r > R \end{cases} \quad (9)$$

Here R denotes the surface radius and M denotes the gravitational mass of the star [22].

It is useful to introduce the nondimensional quantities

$$\bar{r} = \frac{r}{R}; \quad \bar{r} = \frac{r}{M}; \quad \bar{t} = \frac{t}{M} \quad (10)$$

and to define the compaction of the star as

$$C = \frac{2M}{R}; \quad (11)$$

Note that C is limited by the well-known Buchdahl limit $C < 8/9$ [18]. With these definitions, the wave eq. (6) now becomes

$$\partial_{\bar{t}\bar{t}} + \partial_{\bar{r}\bar{r}} = \nabla^2(r) \quad (12)$$

where we have also used $\nabla^2(r) = M^{-2} \nabla^2(r)$. In the following we will drop the tildes again, and it will be understood that all variables are nondimensional. This is equivalent to setting $M = 1$.

Adopting the notation of Chandrasekhar and Ferrari [13],

$$y = \frac{1}{1 - C^3 r^2}; \quad y_1 = \frac{1}{1 - C}; \quad (13)$$

the generalized potential $V(r)$ can be written

$$V(r) = \begin{cases} \frac{3y_1 - y}{4} - \frac{(\lambda + 1)}{r^2} (3y_1 - y) + \frac{C^3}{4} (2y - 3y_1) & r < 2=C \\ 1 - \frac{2}{r} - \frac{(\lambda + 1)}{r^2} + \frac{2}{r^3} & r > 2=C \end{cases} \quad (14)$$

In the exterior of the star $r > 2=C$ the potential reduces to the Schwarzschild potential. Note also that the potential is discontinuous at the surface of the star ($r = 2=C$). The size of the discontinuity is $3C^3(1 - C) = 8$, independent of λ . In Figure (1) we show $V(r)$ for different values of the compaction for $\lambda = 0$ and $\lambda = 1$.

C. The Generalized Tortoise Coordinate

We now have to integrate eq. (4) to find an expression for the generalized tortoise coordinate r . For $r > 2=C$, the integration

$$r = e^{\int \frac{dr}{1 - 2/r}} \quad (15)$$

yields the familiar Schwarzschild tortoise coordinate

$$r = r + 2 \ln\left(\frac{r}{2} - 1\right) \quad (16)$$

(where a constant of integration has been chosen appropriately).

In the interior, $r < 2=C$, we have to integrate

$$r = \int \frac{2 dr}{y(3y_1 - y)}; \quad (17)$$

With the substitution

$$s = \frac{1}{3y_1 - y}; \quad (18)$$

the integrand can be brought into the form

$$r = \frac{4}{C^{3/2}} \int \frac{ds}{(y^2 s^2 + 6y_1 s - 1)^{1/2}}; \quad (19)$$

where we have used

$$y_2 = 8 - 9C; \quad (20)$$

The integration can now be carried out analytically and yields

$$r = \frac{4}{(C^3 y_2)^{1/2}} \arcsin \left(\frac{y_2}{3y_1 - y} + 3y_1 \right) + \arcsin \left(\frac{y_2}{2y_1} + 3y_1 \right) + \frac{2}{C} + 2 \ln\left(\frac{1}{C} - 1\right); \quad (21)$$

where the dependence on r enters through y , and where we have chosen a constant of integration such that r is continuous across the surface of the star. As expected, we recover $r = r + 1$ in the Newtonian limit $C \rightarrow 0$. In the ultrarelativistic limit $C \rightarrow 8/9$, r at the origin $r = 0$ approaches negative infinity, $r(0) \rightarrow -1$. Since r measures the coordinate time which elapses along a photon radial geodesic (eq. (12)), this implies that the light travel time between the surface and the center of the star grows without bound as the star's compaction reaches the Buchdahl limit. This property has important consequences for the scattering of waves from ultrarelativistic stars, as we will discuss in Sec. III. In Fig. 2, we show r as a function of r for various different compactifications C .

D. Numerical Implementation

We integrate eq. (12) numerically using the finite-differencing scheme described by Gundlach, Price and Pullin [3], which is based on the double null coordinates

$$u = t - r; \quad v = t + r; \quad (22)$$

In terms of these, eq. (12) becomes

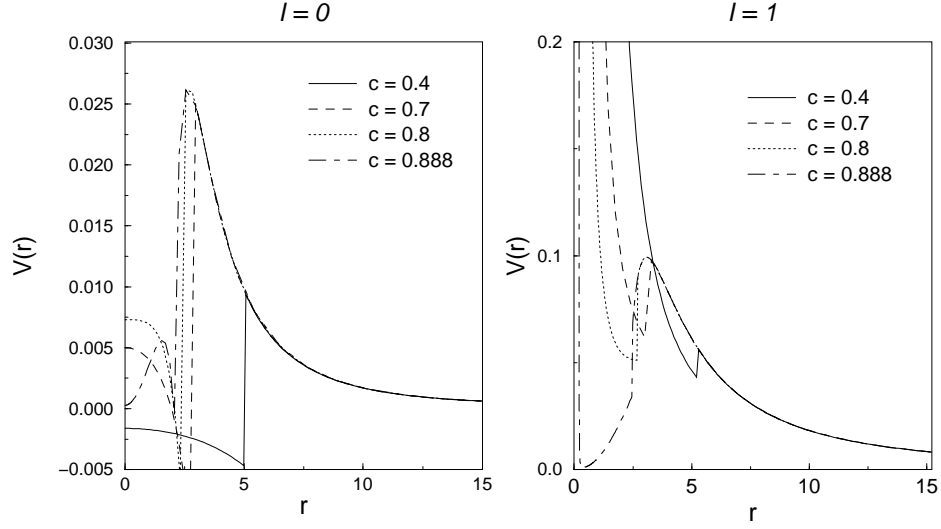


FIG. 1. The potential inside and outside of the star for different values of the compactness $C = 2M/R$. Note the discontinuity at the stellar surface.

$$4_{,uv} = V_{,}(r) : \quad (23)$$

Denoting

$$u_+ = u + \Delta u ; \quad v_+ = v + \Delta v ; \quad (24)$$

where Δ is the grid spacing, we can write a finite difference equation for eq. (23) as

$$(u_+; v_+) = 1 - \frac{\Delta^2}{8} V_{,}(r) \left((u_+; v) + (u; v_+) \right) \quad (25)$$

Here r can be found from $r = (v - u)/2$ by numerically inverting eq. (21). We impose a regularity boundary condition at the origin ($\Delta = 0$ at $r = 0$) and an outgoing wave boundary condition

$$(u_+; v_+) = (u_+; v) \quad (26)$$

at a large radius $r = r_{\text{max}}$ in the asymptotically flat regime.

We tested our code in various ways. For a vanishing potential $V_{,}(r) \rightarrow 0$ at space and $\Delta = 0$, the analytical scalar wave solution is reproduced exactly. For smooth potentials (as for a Schwarzschild black hole), the code produces second order accurate results ($O(\Delta^2)$). This

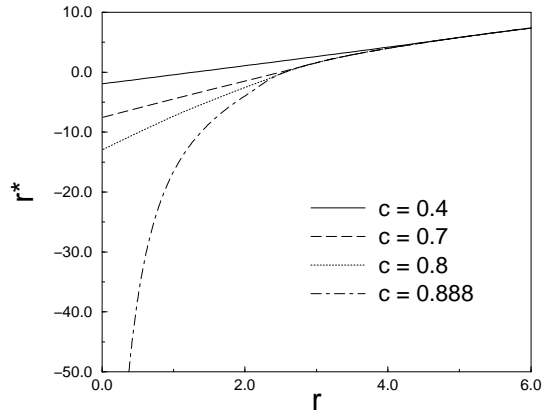


FIG. 2. The tortoise coordinate r^* as a function of r for several different values of C .

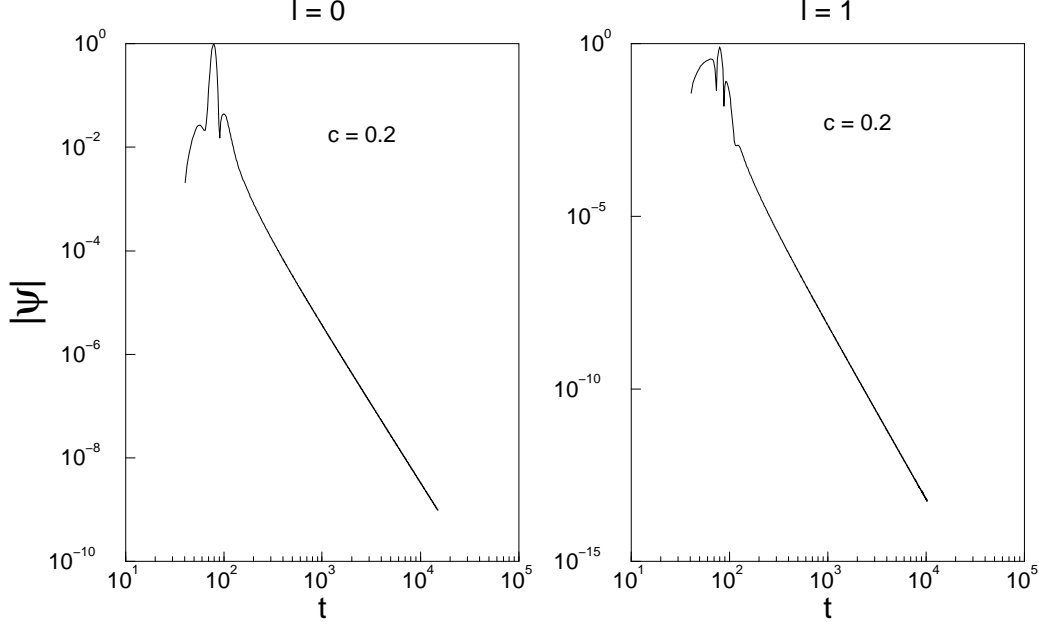


FIG. 3. Late-time behaviour for the $l = 0$ and $l = 1$ modes with $C = 0.2$. For such low values of the compaction we observe a power-law decay in a nearly Newtonian exterior geometry.

second order convergence is broken by the discontinuity in the potential at the surface of the star, but the code is still convergent. We also convinced ourselves that by smoothing out the discontinuity, second order convergence is restored. Lastly, we checked that our evolution scheme conserves energy, which is discussed in more detail in Appendix A.

Following [6], we choose as initial data $(u;0) = 0$ and $(0;v) = \exp(-(v-y)^2/(2\sigma^2))$ for $v_c = 30$ and $\sigma = 3$. However, the qualitative features of our findings should be independent of this particular choice. All results will be shown as a function of time $t = \frac{1}{2}(v+u)$ for an observer at fixed radius $r = 50$.

III. NUMERICAL RESULTS

We focus on the late-time radiative falloff of the scalar field, and find that three different regimes of neutron star compaction which can be clearly distinguished. We discuss these different regimes below, and summarize our numerical results in Table I.

For small compactness we observe a power-law decay

$2M/R$	$r(0)$	$r(R)$	$(l=0)$	$(l=1)$
0.2	0.704	12.773	-3.01	-5.02
0.83	-16.799	-0.762	-3.01	-5.02
0.882	-55.947	-1.755	-3.00	
0.888	-163.039	-1.889	-3.01	
0.8888	-525.380	-1.907	-3.01	

TABLE I. Summary of different runs. We tabulate the compaction $C = 2M/R$, the value of the tortoise coordinate at the origin $r(0)$ and the surface of the star $r(R)$, and the slope of the late-time power law tail for $l=0$ and $l=1$. For $l=0$ with $C = 0.888$ and $C = 0.8888$, the slopes refer to the power law decay before the arrival of the first of the periodic peaks. The accuracy of the slopes is limited by the finite integration time.

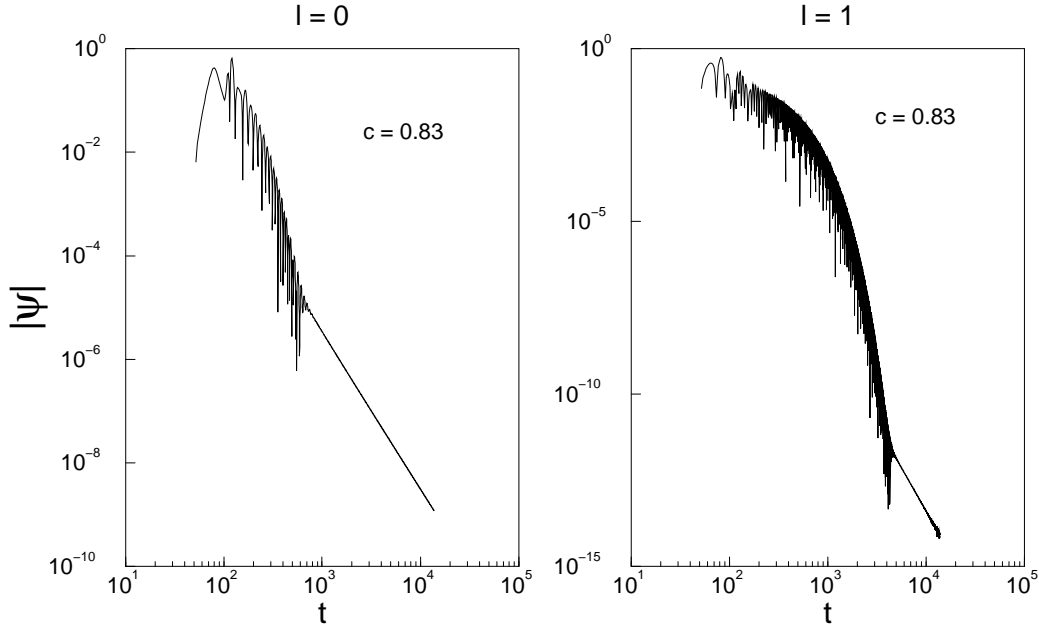


FIG. 4. Late-time behaviour for the $l = 0$ and $l = 1$ modes with $C = 0.83$. Both modes are in the intermediate compaction regime where trapped quasi-normal modes are excited and are observed to decay exponentially.

in a nearly Newtonian (exterior) Schwarzschild geometry. The initial pulse is reflected at the origin and then propagates outward, leaving behind the power-law decay $\propto t^{-2/3}$ from backscattering off the weak spacetime curvature at large radii. The slope of this power-law is consistent with the value $(2/3)$ predicted for backscatter in any spherically symmetric, static, asymptotically flat spacetime [3]. As a typical example, we show results for $C = 0.2$ for both $l = 0$ and $l = 1$ in Fig. 3. This behaviour is observed for compactions C up to about 0.8 for the $l = 0$ mode and 0.7 for the $l = 1$ mode.

At these high compactions, we find a smooth transition into an intermediate regime. Once the star is sufficiently compact, a sufficiently deep potential well forms between the peak of the exterior Schwarzschild potential and the origin (see Fig. 1), and the incoming pulse can excite quasi-normal modes trapped in this potential well. These modes decay exponentially as their energy slowly “leaks” out to infinity. Once their amplitude has dropped to small enough values, the power-law tail emerges and dominates the late-time decay of the field. In Fig. 4, we demonstrate this behavior for $C = 0.83$.

Note that due to the discontinuity of the potential,

there is a small potential well just inside the surface of the star for all compactions C . For small compactions, however, this well is too small to excite quasi-normal modes, and it is only when the surface of the star is close to the maximum of the exterior Schwarzschild potential that this potential well becomes sufficiently large (compare Fig. 1) to observe the exponential decay.

A third kind of behaviour is observed in the strongly relativistic regime, when the compaction of the star is $C > 0.86$ for $l = 0$ and $C > 0.83$ for $l = 1$. Here the early part of the decay of the initial pulse is dominated by quasiperiodic peaks with a period approximately equal to twice the light travel time between the maximum of the exterior effective potential and the origin. Recall that for increasingly large compactions, the origin is pushed to larger negative values of r , thereby increasing the width of the potential well. For sufficiently large compactions, the wavelength of the incoming pulse is smaller than the width of the potential well. Instead of exciting a quasi-normal mode, it oscillates between the origin, where it is completely reflected, and the maximum of the external Schwarzschild potential, where it is partially reflected. Every time the pulse reaches the latter, a small part of

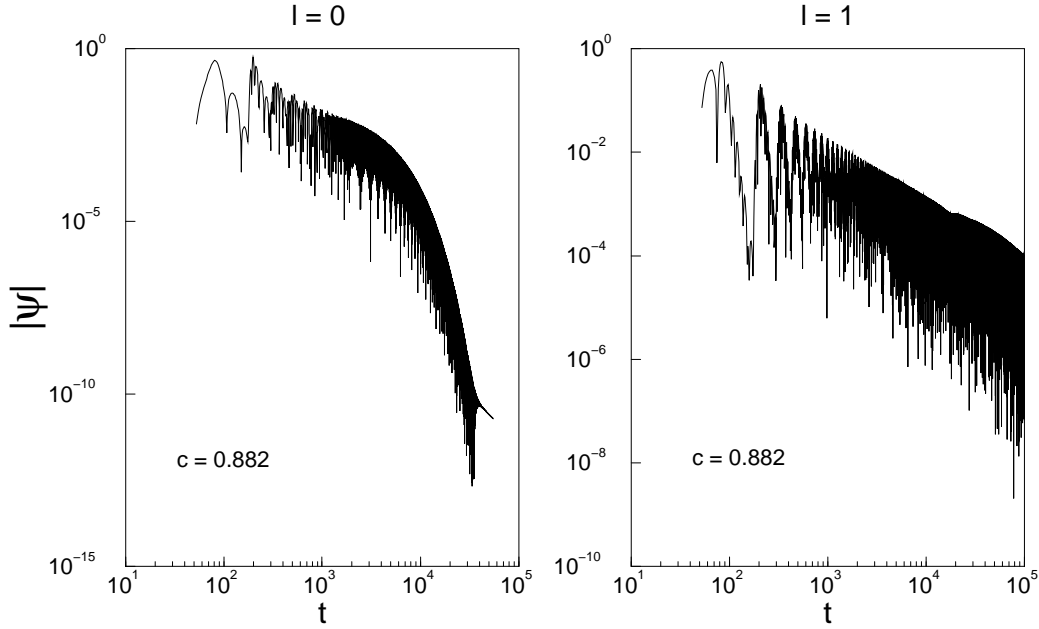


FIG. 5. Late-time behaviour for the $l = 0$ and $l = 1$ modes with $C = 0.882$. Both modes are in the strongly relativistic regime, where the early part of the decay is dominated by almost periodic peaks. In the case of the $l = 0$ mode we can also see how the exponential decay of quasi-normal modes is recovered in later times, to eventually give rise to the power-law tail.

it will be transmitted as one of the quasi-periodic peaks which we observe at large radii.

During its travel in the non-zero potential background within the well and with each reflection at the barrier, the pulse is distorted and becomes broader with time. This effect makes the observed pattern quasi-periodic as opposed to periodic. Once the typical wavelength becomes comparable with the width of the well, we can no longer cleanly separate individual peaks. Simultaneously, the exponential decay found in the intermediate regime is recovered, suggesting that once the pulse "fills out" the well, the dynamics can again be described by an exponentially decaying quasi-normal mode. Ultimately, a power-law tail again emerges for very late times. We show this behavior for $C = 0.882$ in Fig. 5. For $l = 1$, the reappearance of the power-law occurs only once the signal has decayed below computer accuracy, which is why we are unable to observe this transition.

An extreme case of the decay pattern described above is exhibited in the case of extremely large compactifications. In this case, as C approaches $8=9$, the light travel time from the maximum of the exterior potential to the origin grows without limit. Thus, the time between the

initial peaks also grows without bound. As a result, we can observe a power-law decay between individual peaks. When the next peak arrives, it dominates over the power-law tail until it decays enough so that the power-law once again emerges. However, since the power-law itself drops to increasingly small amplitudes, and since the peaks broaden and eventually overlap, the power-law tail is temporarily lost, to re-emerge only at very late times, when periodic peaks and subsequent exponential decay have decayed sufficiently so that the power-law tail becomes once again the dominant pulse remnant. The early part of this behaviour for $l = 0$ and for compactions $C = 0.888$ and $C = 0.8888$ is shown in Fig. 6.

In the limit $C \rightarrow 8=9$, the light travel time between potential maximum and origin becomes infinite and hence the first pulse will arrive infinitely late. Thus, in the Buchdahl limit we recover the characteristic power-law decay of a black hole spacetime.

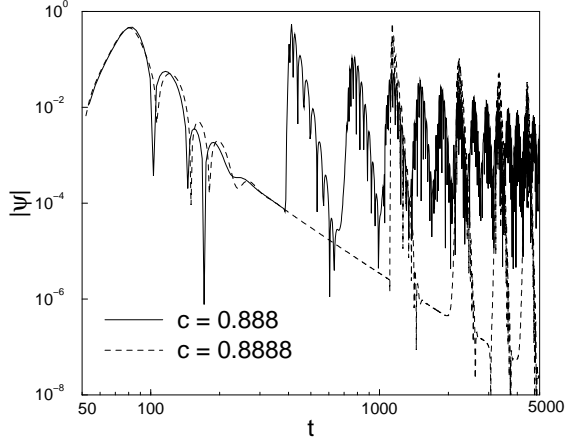


FIG. 6. Late-time behavior for $\lambda = 0$ for stars with extremely large compactions. The decaying field has enough time to enter the power-law tail before the first of the quasiperiodic pulses arrives. Note that as the compaction increases, the first pulse arrives at increasingly late times.

IV. SUMMARY

We study the backscattering of scalar waves off uniform density neutron stars, varying the compaction of the neutron star from the Newtonian limit $2M/R = 1$ to the ultrarelativistic Buchdahl limit $2M/R = 8/9$, and focussing on the excitation of quasi-normal modes and the emergence of power-law tails. We find that three distinct regimes in the compaction can be identified.

In the Newtonian regime, the response is dominated by a reflection of the initial pulse off the center of the star, and subsequent power-law falloff. In an intermediate regime, more quasi-normal modes of the neutron star are excited, which decay exponentially and ultimately drop in amplitude below the power-law tail, which dominates the late-time falloff. In the highly relativistic regime, in which the light travel time between the center of the star and the maximum of the curvature potential increases to large values, the initial wave package bounces back and forth between those two and gives rise to quasi-periodic signals. Between these quasi-periodic signals, the field decays following a power-law. In the ultrarelativistic limit, the light travel time reaches infinity, and the initial wave signal will never reach the center of the star. The modes of neutron stars can therefore no longer be excited, and it is in this sense that the late-time radiative decay from ultrarelativistic neutron stars loses all its features and again gives rise to power-law tails. By tracking the scattered wave amplitude, a distant observer can distinguish whether the central object is a black hole or a neutron star, and if the latter, can determine the compaction of the star.

The authors gratefully acknowledge useful conversations with Eric Poisson. This work was supported by NSF Grants AST 96-18524 and PHY 99-02833 and NASA Grant NAG 5-7152 at Illinois.

APPENDIX A: CONSERVATION OF ENERGY

In this appendix we derive a conserved energy integral which can be used as a test of the numerical simulation.

Since the spacetime (1) is static, there exists a Killing vector $\tilde{\omega} = \partial/\partial t$. Thus, a conserved current can be constructed by contracting $\tilde{\omega}$ with the stress energy tensor T ,

$$J = T \cdot \tilde{\omega} \quad (A1)$$

The conservation of J implies $J_{;\alpha} = 0$ or, by integrating over a 4-volume V ,

$$\int_V g^{1=2} J_{;\alpha} dx^\alpha = 0 \quad (A2)$$

Applying Gauss's theorem, eq. (A2) yields

$$\int_V J_{;\alpha} dx^\alpha = 0 \quad (A3)$$

where V denotes the closed 3-surface enclosing the 4-volume V . The surface element is given by $d^3x = 1/3! g^{1=2} dx^1 dx^2 dx^3$, where ϵ^{123} is the Levi-Civita alternating symbol. In the following we choose V to be the volume defined by $0 \leq r \leq r_0$ and $t_0 \leq t \leq t_1$, so that eq. (A3) can be written as

$$\int_{r_0}^{\infty} \int_{t_0}^{t_1} J_{;\alpha} dx^\alpha = \int_{r=r_0}^{\infty} \int_{t_0}^{t_1} J^r dx^t dx^\theta dx^\phi : \quad (A4)$$

Here the left hand side represents the difference in energy interior to a spherical volume between two instants of time t_0 and t_1 , and the right hand side represents the integrated flux through the surface of the volume at $r = r_0$ during that time interval.

For a massless scalar wave the stress energy tensor is

$$T_{\alpha\beta} = \frac{1}{4} [\dot{\phi}^2 g_{\alpha\beta} - 2 \phi_{;\alpha} \phi_{;\beta}] \quad (A5)$$

so that the relevant components of the flux $J = T_{\alpha\beta} \tilde{\omega}^\alpha$ become

$$J^0 = \frac{1}{8} \left(\dot{\phi}^2 + e^{2\phi} \phi_{;r}^2 + \frac{1}{r^2} \phi_{;\theta}^2 + \frac{1}{r^2 \sin^2 \theta} \phi_{;\phi}^2 \right) \quad (A6)$$

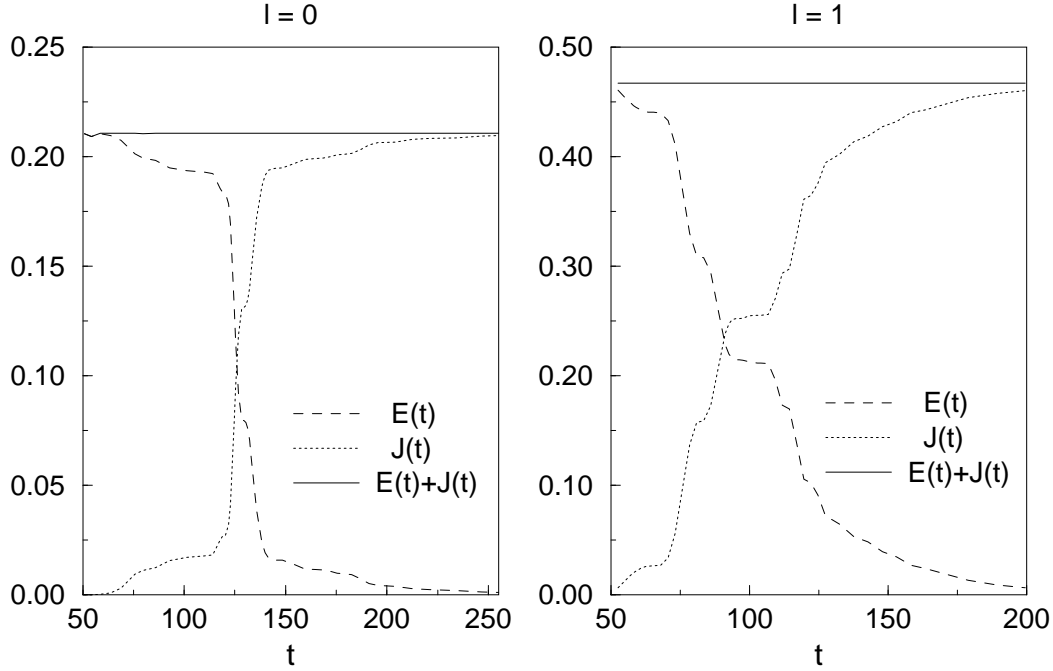


FIG. 7. Energy conservation for $l = 0$, $C = 0.85$ and for $l = 1$, $C = 0.8$. We plot the total energy $E(t)$ contained within $r = 50$, the integrated flux $J(t)$ across $r = 50$, and the sum, which has to be equal to $E(0)$, a constant.

and

$$J^r = \frac{1}{4} e^{2\gamma} \gamma_{,r} \gamma_{,0} \quad (A 7)$$

In the following we will consider an axisymmetric mode ($m = 0$), for which all derivatives with respect to φ vanish.

Inserting the fluxes together with the determinant of the metric $\gamma_{ij}^{j=2} = e^{2\gamma} \sin^2 \theta$ into eq. (A 4) and performing the integration over θ then yields

$$\begin{aligned} \frac{1}{2} \int_0^Z dr dr^2 e^{2\gamma} \gamma_{,0}^2 + e^{2\gamma} \gamma_{,r}^2 + \frac{e^{2\gamma}}{r^2} \gamma_{,i}^2 &= \int_{t_0}^{t_1} dt \int_{r=r_0}^{\infty} dr r^2 \gamma_{,r} \gamma_{,0} e^{2\gamma} \end{aligned} \quad (A 8)$$

where we have used $\sin^2 \theta = \cos^2 \theta$. The limits of integration in eq. (A 8) are from $r = 0$ to r_0 , from $t = t_0$ to t_1 and from $\theta = 0$ to π .

We can now define $E(t)$ as the energy inclosed within a sphere of radius r_0 at time t ,

$$E(t) = \frac{1}{2} \int_0^Z dr dr^2 e^{2\gamma} \gamma_{,0}^2 + e^{2\gamma} \gamma_{,r}^2 + \frac{e^{2\gamma}}{r^2} \gamma_{,i}^2 \quad (A 9)$$

(with the same limits of integration as in eq. A 8), and $J(t)$ as the outgoing flux of energy through the surface of the same sphere integrated over the surface of this sphere and over the time interval t_0 to t_1 ,

$$J(t) = \int_{t_0}^{t_1} dt \int_{r=r_0}^{\infty} dr r^2 \gamma_{,r} \gamma_{,0} e^{2\gamma} \quad (A 10)$$

Eq. (A 8) can now be rewritten

$$E(t) + J(t) = E(t_0) = \text{const} \quad (A 11)$$

The expression for the energy and flux integrals can be further simplified by decomposing γ into spherical harmonics

$$\gamma(t; r; \theta; \varphi) = \gamma_l(t; r) Y_{lm}(\theta; \varphi) \quad (A 12)$$

as we do in our dynamical evolution.

For the spherically symmetric case $l = 0$, $Y_{00} = 1/\sqrt{4\pi}$, the energy integral (A 9) becomes

$$E_0(t) = \frac{1}{4} \int_0^{r_0} dr r^2 e^{2\gamma} \gamma_{,0}^2 + e^{2\gamma} \gamma_{,r}^2 \quad (A 13)$$

and the flux integral (A 10)

$$J_0(t) = \frac{1}{2} \int_{t_0}^{t_1} dt \int_{r=r_0}^{\infty} dr r^2 \gamma_{,r} \gamma_{,0} e^{2\gamma} \quad (A 14)$$

For $\ell = 1$ and $m = 0$ we have $Y_{10} = \sqrt{\frac{3}{4\pi}}$, and eqs. (A 9) and (A 10) now become

$$E_1(t) = \frac{1}{4} \int_0^{r_0} r^2 e^{-\frac{1}{2} \int_0^r \omega^2 dr} + e^{-\frac{1}{2} \int_0^r \omega^2 dr} + \frac{1}{2} \int_0^{r_0} e^{-\frac{1}{2} \int_0^r \omega^2 dr} \omega^2 dr \quad (\text{A } 15)$$

and

$$J_1(t) = \frac{1}{2} \int_{t_0}^t r^2 \omega_{,r} \omega_{,0} e^{-\frac{1}{2} \int_0^r \omega^2 dr} dt \quad (\text{A } 16)$$

Energy conservation in our dynamical code can now be checked by verifying that eq. (A 11) is satisfied at all times. In Fig. (7) we show the energy and flux integrals for examples with $\ell = 0$ and $\ell = 1$. The sum of the two integrals remains constant with an accuracy which increases with increasing grid resolution, implying that energy is indeed conserved.

- [18] H. A. Buchdahl, Phys. Rev. 116, 1027 (1959); also *Seventeen Simple Lectures on General Relativity* (Wiley, New York, 1981).
- [19] N. Andersson, and K. D. Kokkotas, Phys. Rev. Lett. 77, 4134 (1996).
- [20] G. Allen, N. Andersson, K. D. Kokkotas, B. F. Schutz, Phys. Rev. D 58, 124012 (1998).
- [21] J. Rou, gr-qc/0003088.
- [22] C. W. Misner, K. S. Thorne and J. A. Wheeler, *Gravitation* (Freeman, New York, 1973); Box 23.2, page 609.

-
- [1] V. de la Cruz, J. E. Chase, and W. Israel, Phys. Rev. Lett. 24, 423 (1970).
 - [2] R. H. Price, Phys. Rev. D 5, 2419 (1972); Phys. Rev. D 5, 2439 (1972).
 - [3] C. Gundlach, R. H. Price, and J. Pullin, Phys. Rev. D 49, 883 (1994); Phys. Rev. D 49, 890 (1994).
 - [4] E. S. C. Ching, P. T. Leung, W. M. Suen, and K. Y. Yung, Phys. Rev. Lett. 74, 2414 (1995).
 - [5] P. R. Brady, C. M. Chambers, W. K. Kavanagh, and P. Laguna, Phys. Rev. D 55, 7538 (1997).
 - [6] P. Brady, C. Chambers, W. Laarakkers, and E. Poisson, Phys. Rev. D 60, 064003 (1999).
 - [7] Interestingly, for non-minimally coupled perturbations $(2 - R)' = 0$ the purely exponential decay at late times becomes oscillatory for coupling constant $\gamma > \gamma_c = 3/16$, cf. [6].
 - [8] K. S. Thorne, and A. Campolattaro, Astrophys. J. 149, 591 (1967); Astrophys. J. 152, 673 (1967).
 - [9] S. L. Detweiler, Astrophys. J. 197, 203 (1975)
 - [10] L. Lindblom, and S. Detweiler, Astrophys. J. Suppl. 53, 73.
 - [11] Y. Kojima, Prog. Theor. Phys. 79, 665 (1988).
 - [12] S. Chandrasekhar and V. Ferrari, Proc. R. Soc. Lond. A 432, 247 (1991).
 - [13] S. Chandrasekhar and V. Ferrari, Proc. R. Soc. Lond. A 434, 449 (1991).
 - [14] K. D. Kokkotas, and B. F. Schutz, Mon. Not. R. Astr. Soc. 255, 119 (1992).
 - [15] M. Leins, H. P. Nollert, and M. H. Soel, Phys. Rev. D, 48, 3467 (1993).
 - [16] N. Andersson, Y. Kojima and K. Kokkotas, Astrophys. J. 462, 855 (1996).
 - [17] K. Kokkotas, and B. G. Schmidt, Living Reviews 1999-2 (1999).